



HAL
open science

Calibration and data consistency in parallel and fan-beam linogram geometries

Laurent Desbat, Rolf Clackdoyle

► **To cite this version:**

Laurent Desbat, Rolf Clackdoyle. Calibration and data consistency in parallel and fan-beam linogram geometries. 2019 IEEE Nuclear Science Symposium and Medical Imaging Conference (NSS/MIC), Oct 2019, Manchester, United Kingdom. pp.1-5, 10.1109/NSS/MIC42101.2019.9059826 . hal-03099405

HAL Id: hal-03099405

<https://hal.science/hal-03099405>

Submitted on 6 Jan 2021

HAL is a multi-disciplinary open access archive for the deposit and dissemination of scientific research documents, whether they are published or not. The documents may come from teaching and research institutions in France or abroad, or from public or private research centers.

L'archive ouverte pluridisciplinaire **HAL**, est destinée au dépôt et à la diffusion de documents scientifiques de niveau recherche, publiés ou non, émanant des établissements d'enseignement et de recherche français ou étrangers, des laboratoires publics ou privés.

Calibration and data consistency in parallel and fan-beam linogram geometries

Laurent Desbat and Rolf Clackdoyle^{*†‡}

January 6, 2021

Abstract

In this work we recall well known results related to the Helgason-Ludwig Data Consistency Conditions (DCCs) of the 2D Radon transform. These DCCs are based on moments of each projection. The center of mass of each projection is the projection of the center of mass of the measured object. This property is very useful for aligning the data in case of misalignments. However reversed projection angles, a global constant shift of the projection angles or a global sinusoidal shift of the line index at each projection angle lead to consistent projection data. Thus these acquisition parameter modifications can not be estimated from DCCs. In this work we propose a generalization of these results to parallel and fan-beam linograms.

1 Introduction

There continues to be increasing interest in geometric calibration procedures for computed tomography, because small misalignments of the projections can dramatically degrade the quality of reconstructed images. Self-calibration, whereby unknown geometric misalignments are corrected concurrently with the production scan is also becoming a popular approach ([1, 6]) although there are still challenges to be overcome.

Self-calibration methods generally appeal to data consistency conditions, because geometric misalignments can break down some kinds of consistency [3, 2]. For example, it is known that the order-1 and order-0 Helgason-Ludwig consistency conditions [7, 5, 8] provide information on the center of mass of the object being imaged. Misaligned projections would then reveal inconsistent information on the center of mass and could possibly provide a criterion for correcting these misalignments. On the other hand, order-0 conditions alone only provide the total mass of the object and would not be useful for detecting misalignments. Several other well-known facts (which are all reviewed below) are that if the projection angle is reversed, a mirror version of the reconstructed image occurs; that a fixed shift in the projection angle will just rotate the

***Author version.**

[†]This work was supported in part by the “Fonds unique interministériel” (FUI) and the European Union FEDER in Auvergne Rhône Alpes (3D4Carm project).

[‡]L. Desbat and R. Clackdoyle are with Univ. Grenoble Alpes, CNRS, Grenoble INP, TIMC-IMAG, 38000 Grenoble, France. e-mail: Laurent.Desbat@univ-grenoble-alpes.fr.

reconstructed image by the same angle, but that a fixed shift in the ray variable produces inconsistent projection data.

Although the most common (2D) tomographic imaging configuration uses parallel or fan-beam projections measured on a circle, linogram geometries, whereby a flat detector is placed opposite fan-beam sources following a linear path are also relevant, particularly for non-medical applications such as non-destructive testing, baggage security scanning, etc.

Here, we present the corresponding data consistency properties for the parallel and fan-beam linogram geometries. We explore the center of mass and total mass considerations, we examine the effect of a constant shift of the projection index or of the ray index, and we consider reversing the projection index. These results provide the corresponding information for linogram self-calibration issues as is known for the conventional circular tomographic model.

The 2D Radon transform corresponds to the circular tomographic model. We begin by expressing the stated (and well-known) results mathematically for this case. Then we take the small step to parallel linogram projections and even there we see some interesting differences (e.g., the rotation of the object becomes a linear shear transformation). Finally we examine the fan-beam linogram projections. These linogram results, derived from known linogram consistency conditions, are new.

2 2D Radon transform

We let $\mu \in \mathbb{L}^1(\mathbb{R}^2)$ represent the 2D object function. We define parallel projections by

$$p_\phi(s) := p(\phi, s) := \mathcal{R}\mu(\phi, s) := \int_{\mathbb{R}} \mu(s\vec{\theta}_\phi + l\vec{\zeta}_\phi) dl \quad (1)$$

where $\phi \in [0, 2\pi)$, $s \in \mathbb{R}$, $\vec{\theta}_\phi = (\cos \phi, \sin \phi)$, $\vec{\zeta}_\phi = (-\sin \phi, \cos \phi)$, so the parallel projection at angle ϕ is p_ϕ . See Fig. 1. We will always use the first variable to indicate the projection index.

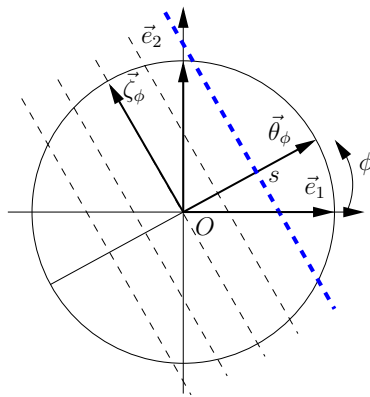


Figure 1: 2D parallel geometry. The line of integration is the dashed blue line $s\vec{\theta}_\phi + \mathbb{R}\vec{\zeta}_\phi$.

The Helgason-Ludwig consistency conditions [8] are expressed in terms of moments of the parallel projections.

$$\Pi_n(\phi) = \forall n \in \mathbb{N}, \int_{\mathbb{R}} s^n p(\phi, s) ds \quad (2)$$

As is well-known, the function p is consistent (meaning that there exists some μ such that $p = \mathcal{R}\mu$) if and only if, $\forall n = 0, 1, 2, \dots, \Pi_n$ is a homogeneous polynomial in $\cos \phi$ and $\sin \phi$ of degree n (or else the zero polynomial). I.e. Π_n is of the form

$$\Pi_n(\phi) = \sum_{k=0}^n a_k \cos^{n-k}(\phi) \sin^k(\phi) \quad (3)$$

which can be alternatively expressed as

$$\begin{aligned} \Pi_n(\phi) = & A_n \cos^n(\phi - A_{n-1}) + A_{n-2} \cos^{n-2}(\phi - A_{n-3}) + \\ & \dots + L \end{aligned} \quad (4)$$

where the last term L is $A_1 \cos(\phi - A_0)$ if n is odd, and A_0 if n is even.

2.1 Mass and center of mass

It is well-known and easily demonstrated that for each projection ϕ , $\Pi_0(\phi)$ is the mass of μ :

$$\begin{aligned} \Pi_0(\phi) &= \int_{\mathbb{R}} p_\phi(s) ds = \int_{\mathbb{R}^2} \mu(s\vec{\theta}_\phi + l\vec{\zeta}_\phi) dl ds \\ &= \int_{\mathbb{R}^2} \mu(\vec{x}) d\vec{x} \end{aligned} \quad (5)$$

Only slightly less well-known is the fact that the center of mass c_ϕ of the ϕ -projection p_ϕ is equal to the ϕ -projection, $\vec{c} \cdot \vec{\theta}_\phi$, of the center of mass $\vec{c} \in \mathbb{R}^2$ of μ . Indeed

$$\begin{aligned} c_\phi &= \frac{\int_{\mathbb{R}} s p_\phi(s) ds}{\int_{\mathbb{R}} p_\phi(s) ds} = \frac{\Pi_1(\phi)}{\Pi_0(\phi)} = \frac{\int_{\mathbb{R}} s \int_{\mathbb{R}} \mu(s\vec{\theta}_\phi + l\vec{\zeta}_\phi) dl ds}{\int_{\mathbb{R}} \int_{\mathbb{R}} \mu(s\vec{\theta}_\phi + l\vec{\zeta}_\phi) dl ds} \\ &= \frac{\int_{\mathbb{R}^2} (\vec{x} \cdot \vec{\theta}_\phi) \mu(\vec{x}) d\vec{x}}{\int_{\mathbb{R}^2} \mu(\vec{x}) d\vec{x}} = \frac{\left(\int_{\mathbb{R}^2} \vec{x} \mu(\vec{x}) d\vec{x} \right) \cdot \vec{\theta}_\phi}{\int_{\mathbb{R}^2} \mu(\vec{x}) d\vec{x}} = \vec{c} \cdot \vec{\theta}_\phi \end{aligned}$$

2.2 Projection index and ray index

Suppose $p = \mathcal{R}\mu$ and now let $p_\Sigma(\phi, s) := p(-\phi, s)$. The corresponding moments are $\Pi_n^\Sigma(\phi) = \Pi_n(-\phi)$ which are also of the required form (Eq. (3)), so they correspond to some function μ_Σ (i.e. $p_\Sigma = \mathcal{R}\mu_\Sigma$). We easily verify that $\mu_\Sigma(x_1, x_2) = \mu(x_1, -x_2)$, which says that if the projection angle is reversed, the reconstructed function is reflected about the x_1 -axis.

Now consider $p_{(\delta,0)}(\phi, s) := p(\phi + \delta, s)$, and we observe that the corresponding moments $\Pi_n^{(\delta,0)}(\phi) = \Pi_n(\phi + \delta)$ are also of the required form (Eq. (4)). The corresponding function μ_δ is obviously just the rotated version $\mu_\delta(x_1, x_2) = \mu(x'_1, x'_2)$ with $x'_1 = x_1 \cos \delta - x_2 \sin \delta$, $x'_2 = x_1 \sin \delta + x_2 \cos \delta$.

This time, shifting the ray index by a constant (instead of the projection index), we define $p_{(0,\delta)}(\phi, s) := p(\phi, s + \delta)$. We find $\Pi_n^{(0,\delta)}(\phi) = \Pi_n(\phi) + n\delta\Pi_{n-1}(\phi) + n(n-1)/2\delta^2\Pi_{n-2}(\phi) + \dots + \delta^n\Pi_0(\phi)$ which is a polynomial in $\sin\phi$ and $\cos\phi$ but it is not homogeneous. So the projections $p_{(0,\delta)}$ are not consistent and do not correspond to any function, which agrees with our intuition that the projections are no longer correctly aligned with each other. However, a sinusoidal shift of the ray index is consistent: $\forall \vec{v} \in \mathbb{R}^2, p(\phi, s + v_1 \cos\phi + v_2 \sin\phi)$ is as consistent as $p(\phi, s)$. Indeed let $\mu_{\vec{v}} := \mu(\vec{x} + \vec{v})$ then $\mathcal{R}\mu_{\vec{v}}(\phi, s) = \mathcal{R}\mu(\phi, s + \vec{v} \cdot \vec{\theta}_\phi)$.

3 Parallel Linograms

We examine the parallel linogram case as a stepping stone to fan-beam linograms. The parallel linogram $\bar{\Gamma}(u, q)$ is defined by

$$\begin{aligned} \bar{\Gamma}_u(\lambda) &:= \bar{\Gamma}(u, q) := \bar{\mathcal{L}}\mu(u, q) \\ &:= \int_{\mathbb{R}} \mu((q, 0) + l(-u, 1)) dl. \end{aligned} \quad (6)$$

The parallel linogram projections are of the form $\bar{\Gamma}_u$ where the linear projection index u specifies the orientation of the projection. See Fig. 2.

Consistency conditions for parallel linograms are easily derived from the Helgason-Ludwig conditions, since the linograms just describe the same projections using different variables [9]. Let $J_n(u)$ be the n^{th} moment of $\bar{\Gamma}_u$:

$$J_n(u) := \int_{\mathbb{R}} \bar{\Gamma}_u(q) q^n dq \quad (7)$$

then $\bar{\Gamma} = \bar{\mathcal{L}}\mu$ for some object μ if and only if, $\forall n$, $J_n(u)$ is a polynomial of degree at most n , i.e. $J_n(u)$ is of the form

$$J_n(u) = b_0 + b_1 u + \dots + b_n u^n \quad (8)$$

3.1 Mass and center of mass

It can be shown directly that for each projection u , $J_0(u)$ is the mass of μ . This property is not obvious because $\bar{\Gamma}(u, q) = \cos\phi p(\phi, s)$ (where $u = \tan\phi$ and $s = q \cos\phi$), and the scaling factor $\cos\phi (= 1/\sqrt{1+u^2})$ would suggest the mass is related to J_0 via some function of u . However, at larger u , the sampling in q is denser, and the combined effect cancels to yield the simple relation

$$\begin{aligned} J_0(u) &= \int_{\mathbb{R}} \bar{\Gamma}_u(q) dq = \int_{\mathbb{R}} \int_{\mathbb{R}} \mu(q - lu, l) dl dq \\ &= \int_{\mathbb{R}^2} \mu(\vec{x}) d\vec{x} \end{aligned} \quad (9)$$

where we have made the change of variables $x_1 = q - lu$ and $x_2 = l$.

The center of mass of the u -projection $\bar{\Gamma}_u$ is

$$c_u := \frac{\int_{\mathbb{R}} \bar{\Gamma}_u(q) q dq}{\int_{\mathbb{R}} \bar{\Gamma}_u(q) dq} = \frac{J_1(u)}{J_0(u)} \quad (10)$$

which is a linear shear mapping of μ with shear factor $-\delta$. Indeed

$$\begin{aligned}\bar{\mathcal{L}}\mu_\delta(u, \lambda) &= \int_0^{+\infty} \mu_\delta(\lambda - lu, l) dl \\ &= \int_0^{+\infty} \mu(\lambda - lu + l\delta, l) dl\end{aligned}$$

thus

$$\bar{\mathcal{L}}\mu_\delta(u, \lambda) = \bar{\mathcal{L}}\mu(u - \delta, \lambda) \quad (15)$$

For the case of the translated ray index, we define $\tilde{\mathbb{I}}(u, q) := \mathbb{I}(u, q + \delta)$. The corresponding moments satisfy $\tilde{J}_n(u) = J_n(u) + n\delta J_{n-1}(u) + \dots + \delta^n J_0(u)$, which is indeed a polynomial in u of degree n or less. So there exists some $\tilde{\mu}$ such that $\tilde{\mathbb{I}} = \bar{\mathcal{L}}\tilde{\mu}$. We find $\tilde{\mu}(x_1, x_2) = \mu(x_1 + \delta, x_2)$, a simple translation of μ by $\delta(1, 0)$. But this is a particular case of the following: with $\mu_{\vec{v}}(x) := \mu(x + \vec{v})$ be a translation of μ of $\vec{v} = (v_1, v_2) \in \mathbb{R}^2$ then we have

$$\begin{aligned}\bar{\mathcal{L}}\mu_{\vec{v}}(u, q) &= \int_{\mathbb{R}} \mu((q + v_1, v_2) + l(-u, 1)) dl \\ &= \int_{\mathbb{R}} \mu((q + v_1, v_2) + (l + v_2)(-u, 1)) dl \\ &= \bar{\mathcal{L}}\mu(u, q + v_1 + v_2u)\end{aligned} \quad (16)$$

4 Fan-Beam Linograms

For fan-beam linograms, we define the linogram data $d(\lambda, t)$ by

$$\begin{aligned}d(\lambda, t) &:= (\mathcal{D}\mu)(\lambda, t) \\ &:= \int_0^{+\infty} \mu((\lambda, D) + l(t - \lambda, -D)) dl\end{aligned} \quad (17)$$

where the projection parameter λ indicates the location (λ, D) of the fan-vertex along the line $x_2 = D$, and the ray-variable t indicates the absolute location along the x_1 -axis, which can be considered as a fixed detector. See Fig. 3. Note that this definition is fundamentally different from that in [9] where the ray variable indicates a point relative to the fan-vertex, as if the detector and fan-vertex (e.g. x-ray source) were a single unit. Consistency conditions for $d(\lambda, t)$ can be found in [4]. Let $K_n(\lambda)$ be the n^{th} moment of $d(\lambda, t)$:

$$\forall n \in \mathbb{N}, K_n(\lambda) = \int_{\mathbb{R}} d(\lambda, t)t^n dt \quad (18)$$

then $d = \mathcal{D}\mu$ for some μ if and only if, $\forall n \in \mathbb{N}$, $K_n(\lambda)$ is a polynomial of degree at most n . In [4], it is shown that

$$K_n(\lambda) = \sum_{k=0}^n \alpha_{n-k, k} \lambda^k \quad (19)$$

where

$$\alpha_{n-k, k} = \binom{n}{k} \int_{\mathbb{R}^2} \mu(x_1, x_2) \frac{x_1^{n-k} D^{n-k} (-x_2)^k}{(D - x_2)^{n+1}} dx_1 dx_2. \quad (20)$$

Because the compact support of μ is included in $\mathbb{R} \times (-\infty, D)$, the singularity term $(D - x_2)^{-(n+1)}$ does not affect the integral.

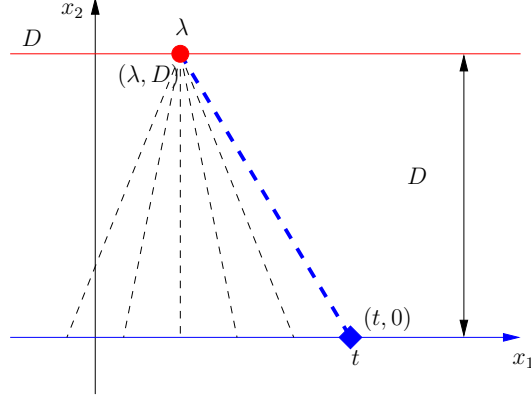


Figure 3: 2D fan-beam linogram tomography. The (half) line of integration $(\lambda, D) + \mathbb{R}^+(x - \lambda, -D)$ is the dashed blue (half) line. The source position is the red point at (λ, D) . The (virtual) detector position is the blue square at $(t, 0)$.

4.1 Mass and center of mass

From (19) and (20) we derive that

$$K_0(\lambda) = \int_{\mathbb{R}^2} \frac{\mu(\vec{x})}{D - x_2} d\vec{x} = \alpha_{0,0}$$

i.e. for each λ -projection, the constant K_0 (independent of λ) equals the total mass of the weighted object function $\frac{\mu(\vec{x})}{D - x_2}$. Note that the object lies under the line $x_2 = D$ and the weight is the inverse distance from $\vec{x} = (x_1, x_2)$ to the line $x_2 = D$.

We also have

$$K_1(\lambda) = \alpha_{1,0} + \alpha_{0,1}\lambda \quad (21)$$

where

$$\alpha_{1,0} = D \int_{\mathbb{R}^2} x_1 \frac{\mu(\vec{x})}{(D - x_2)^2} d\vec{x} \quad (22)$$

$$\alpha_{0,1} = - \int_{\mathbb{R}^2} x_2 \frac{\mu(\vec{x})}{(D - x_2)^2} d\vec{x} \quad (23)$$

Let us define μ_W , the function μ weighted by $\frac{1}{(D - x_2)^2}$

$$\mu_W(\vec{x}) := \frac{\mu(\vec{x})}{(D - x_2)^2}$$

We note that

$$K_0 = \left(\int_{\mathbb{R}^2} \mu_W(\vec{x}) d\vec{x} \right) (D - c_{W2})$$

where $\vec{c}_W = (c_{W1}, c_{W2})$ the center of mass of μ_W , i.e.

$$c_{W1} := \frac{\int_{\mathbb{R}^2} x_1 \mu_W(\vec{x}) d\vec{x}}{\int_{\mathbb{R}^2} \mu_W(\vec{x}) d\vec{x}}$$

and

$$c_{W2} := \frac{\int_{\mathbb{R}^2} x_2 \mu_W(\vec{x}) d\vec{x}}{\int_{\mathbb{R}^2} \mu_W(\vec{x}) d\vec{x}}$$

It can easily be shown that

$$\begin{aligned} \int_{\mathbb{R}^2} \mu_W(\vec{x}) d\vec{x} &= \frac{\alpha_{0,0} - \alpha_{0,1}}{D} \\ c_{W1} &= \frac{\alpha_{1,0}}{\alpha_{0,0} - \alpha_{0,1}} \\ c_{W2} &= -\frac{D\alpha_{0,1}}{\alpha_{0,0} - \alpha_{0,1}} \end{aligned}$$

From Eq. (21), (22) and (23)

$$K_1(\lambda) = ((D, -\lambda) \cdot \vec{c}_W) \int_{\mathbb{R}^2} \mu_W(\vec{x}) d\vec{x}. \quad (24)$$

Now, for an arbitrary point (x_1, x_2) , the λ -projection of this point is given by $t_\lambda(x_1, x_2) = (x_1, x_2) \cdot (D, -\lambda)/(D - x_2)$. Indeed, $\frac{t_\lambda(x_1, x_2) - \lambda}{x_1 - \lambda} = \frac{D}{D - x_2}$, see Fig. 4. Therefore, the center of mass of the λ -projection is the λ -projection of the center of mass of the *weighted* object μ_W . Expressed with moments:

$$\frac{K_1(\lambda)}{K_0} = \vec{c}_W \cdot (D, -\lambda)/(D - c_{W2}). \quad (25)$$

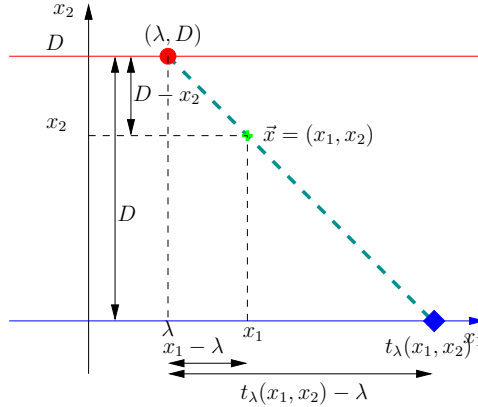


Figure 4: $t_\lambda(x_1, x_2)$ is λ -projection of the point (x_1, x_2) . Thus $\frac{t_\lambda(x_1, x_2) - \lambda}{x_1 - \lambda} = \frac{D}{D - x_2}$.

4.2 Projection index and ray index

Following the pattern of the previous sections, we define $d_\Sigma(\lambda, t) = d(-\lambda, t)$; $d_\delta(\lambda, t) = d(\lambda + \delta, t)$; $\tilde{d}(\lambda, t) = d(\lambda, t + \delta)$. Assuming $d(-\lambda, t) = (\mathcal{D}\mu)(\lambda, t)$, then all three modified fan-beam linograms are also consistent, by the same

arguments as in section 3.2. There exists therefore, μ_Σ , μ_δ , $\tilde{\mu}$ such that $d_\Sigma = \mathcal{D}\mu_\Sigma$, $d_\delta = \mathcal{D}\mu_\delta$, $\tilde{d} = \mathcal{D}\tilde{\mu}$. We find

$$\mu_\delta(\vec{x}) = \mu(\mathbf{A}_\delta \vec{x}) \text{ where } \mathbf{A}_\delta := \begin{bmatrix} 1 & \delta/D \\ 0 & 1 \end{bmatrix}$$

or more simply $\mu_\delta(x_1, x_2) = \mu(x_1 + (\delta/D)x_2, x_2)$. We can easily derive $\tilde{\mu}(x_1, x_2) = \mu(x_1 - (\delta/D)x_2 + \delta, x_2)$, so a constant shift of either the projection index or the ray variable corresponds to a shear of the object.

The expression for μ_Σ is more complex. We show

$$\mu_\Sigma(x_1, x_2) = \left(\frac{D}{2x_2 - D} \right)^2 \mu \left(\frac{D}{2x_2 - D} (-x_1, x_2) \right) \quad (26)$$

$$\begin{aligned} & (\mathcal{F}_D \mu_\Sigma)(\lambda, t) \\ &= \int_0^{+\infty} \mu_\Sigma((\lambda, D) + l(t - \lambda, -D)) dl \\ &= \int_0^{+\infty} \mu_\Sigma(\lambda + l(t - \lambda), D(1 - l)) dl \\ &= \int_0^{+\infty} \left(\frac{1}{1 - 2l} \right)^2 \mu \left(\left(\frac{-\lambda(1 - l) - lt}{1 - 2l}, D \frac{1 - l}{1 - 2l} \right) \right) dl \end{aligned}$$

Assume now that $\text{supp}(\mu)$, the support of μ , is such that $\text{supp}\mu \subset \mathbb{R} \times (-\infty, D/2)$

$$\begin{aligned} & (\mathcal{F}_D \mu_\Sigma)(\lambda, t) \\ &= \int_0^{+\infty} \left(\frac{1}{1 - 2l} \right)^2 \mu \left(\left(\frac{-\lambda(1 - l) - lt}{1 - 2l}, D \frac{1 - l}{1 - 2l} \right) \right) dl \\ &= \int_{1/2}^{+\infty} \left(\frac{1}{1 - 2l} \right)^2 \mu \left(\left(\frac{-\lambda(1 - l) - lt}{1 - 2l}, D \frac{1 - l}{1 - 2l} \right) \right) dl \end{aligned}$$

now the change of variable $1 - u = \frac{1-l}{1-2l}$ or $u = \frac{-l}{1-2l}$, thus $du = \frac{1}{(2l-1)^2} dl$. is one to one between $l \in (1/2, +\infty)$ and $u \in (1/2, +\infty)$. Thus

$$\begin{aligned} (\mathcal{F}_D \mu_\Sigma)(\lambda, t) &= \int_{1/2}^{+\infty} \mu \left((-\lambda(1 - u) + ut, D(1 - u)) \right) du \\ &= (\mathcal{F}_D \mu)(-\lambda, t) \end{aligned} \quad (27)$$

5 Discussion

We have studied five well-known properties of the Radon transform in the context of parallel and fan-beam linograms, and seen remarkable differences and similarities. For example, the center of mass of the 2D Radon parallel projection p_ϕ , respectively the parallel linogram projection $\bar{\Gamma}_u$, is the ϕ -projection, respectively the u -projection, of the center of mass of the measured object μ .

Similarly, the center of mass of the fan beam linogram projection d_λ is the λ -projection of the center of mass of μ_W where $\mu_W(\vec{x}) = \frac{\mu(\vec{x})}{(D-x_2)^2}$. Offsetting the projection index for the Radon transform corresponds to rotating the object, whereas for linograms, it corresponds to performing a shear transformation on the object, see Fig. 5.

We have recalled for the 2D Radon data p and shown for $\bar{\Gamma}$ (parallel linogram data) and d (fan-beam linogram data) that

- $\forall \vec{v} \in \mathbb{R}^2, p(\phi, s + \vec{v} \cdot \vec{\theta}_\phi), p(-\phi, s)$ and $p(\phi + \delta, s)$ are as consistent as $p(\phi, s)$
- $\forall \vec{v} \in \mathbb{R}^2, \bar{\Gamma}(u, \lambda + \vec{v} \cdot (1, u)), \bar{\Gamma}(-u, \lambda), \bar{\Gamma}(u + \delta, \lambda)$ are as consistent as $\bar{\Gamma}(u, \lambda)$.
- $d(\lambda, t + \delta), d(-\lambda, t)$ and $d(\lambda + \delta, t)$ are as consistent as $d(\lambda, t)$.

We have given the respective transforms on μ to obtain the respective consistent data, assuming respectively $p = \mathcal{R}\mu, \bar{\Gamma} = \bar{\mathcal{L}}\mu, d = \mathcal{D}\mu$. As in [3], this information (δ, \vec{v} , the “direction” of the projection acquisition, i.e., the global sign of the respective projection parameter ϕ, u, λ) can not be estimated from the DCCs.

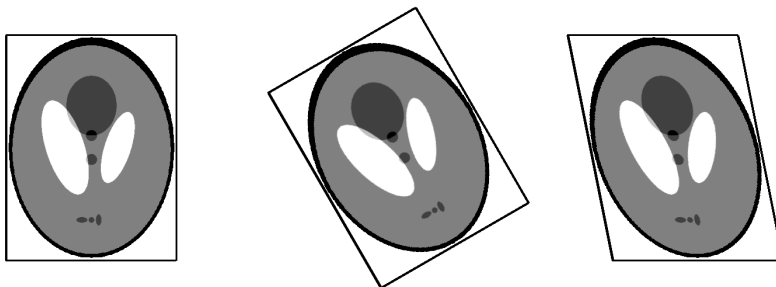


Figure 5: Example of effect of constant offset applied to the projection variable. Left: $\mu(x_1, x_2)$ is the standard Shepp-Logan phantom. Middle: Rotation due to Radon projections offset by a constant shift. Right: Shear transformation due to linogram projections offset by a constant shift.

References

- [1] A. Aichert, M. Berger, J. Wang, N. Maass, A. Doerfler, J. Hornegger, and A.K. Maier. Epipolar consistency in transmission imaging. *IEEE Transactions on Medical Imaging*, 34(11):2205–2219, Nov 2015.
- [2] S. Basu and Y. Bresler. Feasibility of tomography with unknown view angles. *IEEE Trans. Image Processing*, 9:1107–1122, 2000.
- [3] S. Basu and Y. Bresler. Uniqueness of tomography with unknown view angles. *IEEE Trans. Image Processing*, 9:1094–1106, 2000.

- [4] R. Clackdoyle. Necessary and sufficient consistency conditions for fanbeam projections along a line. *IEEE Trans.Nucl.Sci.*, 60:1560–1569, 2013.
- [5] S. Helgason. *The Radon Transform*. Boston, MA, USA: Birkhäuser, 1980.
- [6] J. Lesaint, S. Rit, R. Clackdoyle, and L. Desbat. Calibration for circular cone-beam ct based on consistency conditions. *IEEE Transaction on Radiation and Plasma Medical Sciences*, 1(6):517–526, 2017.
- [7] D. Ludwig. The radon transform on euclidean space. *Commun. Pure Appl. Math.*, 19:49–81, 1966.
- [8] F. Natterer. *The Mathematics of Computerized Tomography*. Wiley, 1986.
- [9] R.Clackdoyle. Data consistency for linograms and planograms. *IEEE Trans Rad Plasma Med*, 4:288–299, 2018.